

Breakdown of Dynamical Scale Invariance in the Coarsening of Fractal Clusters

Massimo Conti

Dipartimento di Matematica e Fisica, Università di Camerino, and Istituto Nazionale di Fisica della Materia, 62032, Camerino, Italy

Baruch Meerson

The Racah Institute of Physics, Hebrew University of Jerusalem, Jerusalem 91904, Israel

Pavel V. Sasorov

Institute of Theoretical and Experimental Physics, Moscow 117259, Russia

We extend a previous analysis [PRL **80**, 4693 (1998)] of breakdown of dynamical scale invariance in the coarsening of two-dimensional DLAs (diffusion-limited aggregates) as described by the Cahn-Hilliard equation. Existence of a second dynamical length scale, predicted earlier, is established. Having measured the “solute mass” outside the cluster versus time, we obtain a third dynamical exponent. An auxiliary problem of the dynamics of a slender bar (that acquires a dumbbell shape) is considered. A simple scenario of coarsening of fractal clusters with branching structure is suggested that employs the dumbbell dynamics results. This scenario involves two dynamical length scales: the characteristic width and length of the cluster branches. The predicted dynamical exponents depend on the (presumably invariant) fractal dimension of the cluster skeleton. In addition, a robust theoretical estimate for the third dynamical exponent is obtained. Exponents found numerically are in reasonable agreement with these predictions.

PACS numbers: 61.43.Hv, 64.60.Ak, 05.70.Fh

I. INTRODUCTION

Nonlinear dissipative systems, driven out of equilibrium, decay to an equilibrium state after the driving agent is switched off or depleted. As long as a freely decaying nonlinear system is far from equilibrium, the relaxation dynamics are non-trivial and it is natural, in simple cases, to look for dynamical scaling and universality. A wide class of nonlinear relaxation problems appears in the context of phase ordering dynamics [1,2]. In the present work we explore a new aspect of phase ordering in systems with a conserved order parameter. This aspect appears when the minority phase has long-range correlations and represents (at least at early times) a fractal cluster (FC). Although such an initial condition does not result from a quench from high to low temperature (a standard setting of phase-ordering dynamics), it is by no means artificial. There are many two-phase systems that exhibit morphological instabilities and ramified growth at an early stage of their dynamics, and coarsening at a later stage. A canonical example is provided by diffusion controlled systems, such as an overcooled liquid or super-saturated solution. The stage of morphological instability and its implications in this system have been under scrutiny [3–7]. If some noise is present, a DLA-like FC develops at this stage [7]. The subsequent surface-tension-driven coarsening of this FC is unavoidable if the system is isolated so that the total amount of available mass or heat is finite. Until recently, this later stage had received only a limited attention. Irisawa *et al.* [8] carried out Monte-Carlo simulations of diffusion-controlled coarsening of a two-dimensional DLA cluster and found a power

law with a non-trivial exponent for the cluster perimeter as a function of time. More recently the first results of investigation of the coarsening of two-dimensional DLA clusters as described by the Cahn-Hilliard (CH) equation were reported [9]. These results are briefly reviewed in the following.

A crucial issue in the theory of phase ordering processes is the presence (or absence) of dynamical scale invariance [1,2]. Dynamical scale invariance implies that there is a single dynamical length scale $\lambda(t)$ such that the coarsening system looks (statistically) invariant in time when lengths are scaled by $\lambda(t)$. It was found Ref. [9] that dynamical scale invariance breaks down during the coarsening of DLA clusters as described by the CH-equation. On the other hand, the coarsening dynamics apparently exhibit *scaling*, by which we mean power laws in time. These power laws (with non-trivial exponents) were found for the cluster perimeter [8,9], and for the dynamical length scale that shows up in the Porod-law part of the equal-time correlation function [9]. We will call this dynamical length scale “the first correlation length”. The absolute values of the dynamical exponents for the cluster perimeter and for the first correlation length are close to each other. The gyration radius of the cluster was found to be constant (within possible logarithmic corrections). The mass dimension of the cluster was also found to be constant (on a shrinking interval of distances). The last two findings indicate that the mass transport is essentially local at this stage of coarsening. We conjectured in Ref. [9] that an additional dynamical length scale (with an exponent larger than that of the first correlation length scale) must show up in the coarsening morphol-

ogy. Furthermore, we speculated that the two different dynamical length scales are the average *width* and *length* of the cluster branches.

Fractal coarsening occurs in many physical systems. Two-dimensional fractal fingering, observed in a Hele-Shaw cell with radial geometry (for a recent review see Ref. [10]), exhibits coarsening at a late stage of the experiment, when forcing of the more viscous fluid by the less viscous fluid stops. Fractal coarsening has been under scrutiny in the context of sintering, in particular of silica aerogels [11–13]. Additional examples are provided by thermal relaxation of initially fractal grain boundaries [14] and by smoothing of fractal polymer structure in the process of polymer collapse [15]. It is interesting, to what extent fractal coarsening is universal.

In this paper we significantly extend the analysis of Ref. [9] of the coarsening of DLA fractals as described by the CH equation. In Section 2 we will report numerical evidence for the existence of an additional dynamical length scale and find the corresponding (second) dynamical exponent. We also introduce in Section 2 an additional measure of the coarsening dynamics: the total “solute mass” content outside the cluster, and find the corresponding (third) dynamical exponent. In the rest of the paper we will try to develop some theoretical understanding of our numerical results. To this end, we consider, in Section 3, the coarsening dynamics of a single slender bar. The results of this analysis are employed in Section 4, where a simple scenario of coarsening of a FC having branching structure is suggested. In this scenario two different dynamical length scales are present: the characteristic width and length of the cluster branches. The corresponding dynamical exponents are calculated; they are found to depend on the (presumably invariant) fractal dimension D of the cluster “skeleton”. A robust theoretical estimate is also obtained for the third (“solute mass”) dynamical exponent. These predictions are in agreement with our numerical results. A change of sign of the third dynamical exponent is predicted at a critical fractal dimension $D_{crit} = 4/3$. Section 5 includes a summary and discussion.

II. COARSENING OF DLA CLUSTERS: NUMERICAL RESULTS

We start with a brief description of our simulations and diagnostics. We solved the (dimensionless) CH equation

$$\frac{\partial u}{\partial t} + \frac{1}{2} \nabla^2 (\nabla^2 u + u - u^3) = 0 \quad (1)$$

numerically by discretizing it on the domain Ω : $0 \leq x \leq 512$, $0 \leq y \leq 512$ with periodic boundary conditions. An explicit Euler integration scheme was used to advance the solution in time, and second order central differences to discretize the Laplace operator. With a mesh size $\Delta x = \Delta y = 1$ no preferred directions emerged in the

computational grid, due to the truncation errors; a time step $\Delta t = 0.05$ was required for numerical stability.

DLA clusters [16] (like the one shown in Fig. 1, upper left), with radius of order 250, were prepared by a standard random-walk algorithm on a two-dimensional square grid and served as the initial conditions for the minority phase $u = 1$. To prevent breakup of the clusters at an early stage of the coarsening process, we followed the technique of Irisawa *et al.* [8] and reinforced the aggregates by an addition of peripheral sites. Comparing the correlation functions before and after the reinforcement, we verified that the reinforcement did not spoil the fractal properties of the cluster.

It is convenient to introduce the density field

$$\rho(\mathbf{r}, t) = \frac{u(\mathbf{r}, t) + 1}{2},$$

which varies between 0 and 1. We identified the cluster as the locus where $u(\mathbf{r}, t) \geq 0$, or $\rho(\mathbf{r}, t) \geq 1/2$. The coarsening process was followed up to a time $t = 5,000$. Typical snapshots of the coarsening process are shown in Fig. 1. One can see that smaller features of the FC are “consumed” by larger features, while the large-scale structure of the cluster is not affected.

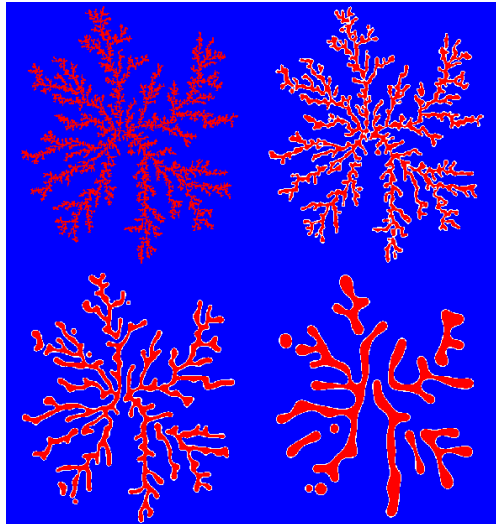


FIG. 1. Coarsening of a DLA fractal cluster as described by the CH-equation. The upper row corresponds to $t = 0$ (left) and 34.7 (right), the lower row to $t = 329.3$ (left) and 4,900 (right).

To characterize the coarsening process, several quantities were sampled and averaged over 10 initial configurations. In this paper we will analyze the following quantities:

1. Gyration radius of the cluster.
2. Circularly averaged equal-time pair correlation function, normalized at $r = 0$:

$$C(r, t) = \frac{\langle \rho(\mathbf{r} + \mathbf{r}', t) \rho(\mathbf{r}', t) \rangle}{\langle \rho^2(\mathbf{r}', t) \rangle}. \quad (2)$$

3. An estimate of the cluster perimeter $P(t)$, defined as the number of broken bonds between the aggregate sites.
4. The “solute mass” outside the cluster:

$$M_s = \int \int_{\rho(\mathbf{r}, t) < 1/2} \rho(\mathbf{r}, t) dx dy. \quad (3)$$

Quantities 2 and 3 were computed after binarization of the phase field data: the value of $\rho = 1$ is attributed to all sites belonging to the cluster, while $\rho = 0$ is attributed to the rest of sites.

As we have already noticed, the gyration radius of the cluster remains constant (within possible logarithmic corrections) until the latest available times, so we will concentrate on the rest of the measurements.

A. Equal-time pair correlation function

An analysis of the r -dependence of the equal-time correlation function at different times shows that coarsening operates only at small and intermediate distances. In the following we will consider separately two regions of distances.

1. Small distances

The linear behavior of the correlation function at small distances (the Porod law), clearly seen in Fig. 2, yields the first correlation length $l_1(t)$ and corresponding dynamical exponent. In a two-phase system with a sharp interface, the first correlation length l_1 is the average minimum distance between a randomly chosen point of the cluster and the interface. We will interpret l_1 as the typical *width* of the cluster’s branches (see Fig. 1).

To determine $l_1(t)$, we approximated $C(r, t)$ on the interval $0.7 \leq C(r, t) \leq 1$ by a linear function $1 - r/l_1(t)$. Fig. 3 shows the inverse correlation length $1/l_1(t)$ versus time, and a corrected-power-law fit

$$\frac{1}{l_1(t)} = \frac{A_{l_1}}{t^\alpha + B_{l_1}}, \quad (4)$$

of this dependence, with

$$\alpha = 0.26, \quad A_{l_1} = 0.44 \quad \text{and} \quad B_{l_1} = 2.0. \quad (5)$$

This fit was obtained on the interval $30 \leq t \leq 2000$ that spans from the time when quasi-equilibrium sharp interfaces have already formed until the time when the system size becomes important (see below). Here and in

the following we do not show the standard deviations of the fitting parameters if they are less than or equal to unity in the last significant digit presented. The dynamical exponent $\alpha = 0.26$ differs from the Lifshitz-Slyozov value of $1/3$ observed in those cases when phase-ordering processes exhibit dynamical scale invariance [1,2,17–21]. In contrast to such processes, no *a priori* form for the correction to the power-law fit for $1/l_1(t)$ is available, so we consider the corrected-power-law fit (4) as empirical. It works well though (see Fig. 3).

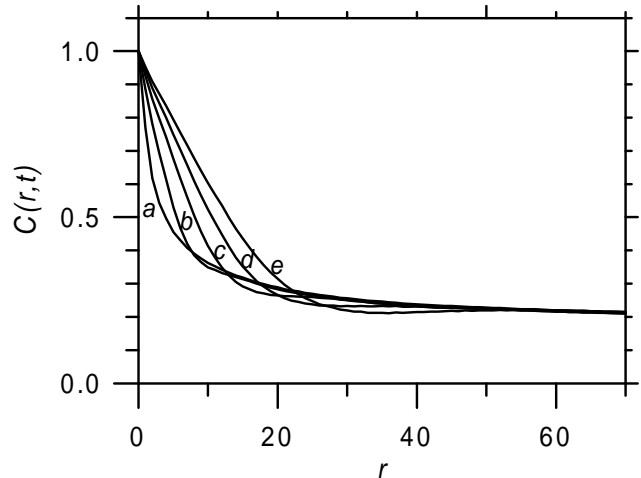


FIG. 2. Dynamics of the equal-time pair correlation function $C(r, t)$ at small and intermediate distances for time moments $t = 0$ (a), 34.7 (b), 516.5 (c), 1992 (d) and 4900 (e).

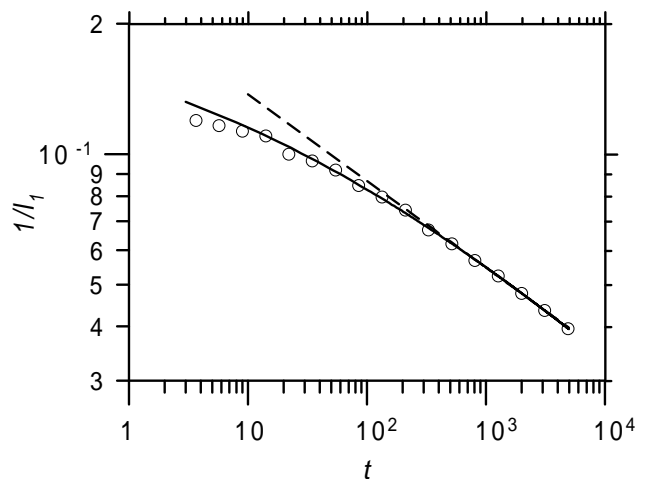


FIG. 3. The inverse first correlation length $1/l_1(t)$ versus time (circles) and its fits (4) (solid line) and (6) (dashed line).

A simpler alternative (chosen in Ref. [9]) is to use a pure power-law fit. For the last decade of time, $490 \leq$

$t \leq 4900$, it gives

$$l_1(t) = C_{l_1} t^\alpha, \quad (6)$$

where

$$\alpha = 0.20 \quad \text{and} \quad C_{l_1} = 4.6. \quad (7)$$

The difference between the values 0.26 and 0.20 is disappointingly large; it gives a measure of the maximum uncertainty of this exponent, caused by systematic errors. Similar uncertainties occur for other dynamical exponents that we find in this work. Our conclusion that α is smaller than the Lifshitz-Slyozov value $1/3$ is unaffected by this uncertainty. In Section 4 we will present a simple coarsening scenario that gives a theoretical prediction for α which agrees, for DLA clusters, with the value 0.26.

2. Intermediate distances

A close inspection of the correlation function $C(r, t)$ at intermediate and large distances show that there are small (within 5 to 10%) changes there. These changes result from small systematic variations of the cluster mass in the process of coarsening (see below). They make it difficult to perform accurate measurements at intermediate and large distances, therefore some normalization at these distances is necessary. We normalized the correlation function $C(r, t)$ at different moments of time to its values at $r = 120$:

$$\hat{C}(r, t) = \frac{C(r = 120, t = 0) C(r, t)}{C(r = 120, t)}. \quad (8)$$

The results obtained by using the normalized function $\hat{C}(r, t)$ are not sensitive to the exact value of r chosen for the normalization, as long as it is large enough.

Figure 4 shows $\hat{C}(r, t)$ at different moments of time. The log-log plot helps to decide on the range of distances and times we can work with. It is seen that $\hat{C}(r, t)$ changes, as a function of time, only at distances smaller than some correlation radius $r_c(t)$ that increases with time. At distances $r > r_c(t)$ $\hat{C}(r, t)$ stays very close to its initial value $C(r, 0)$. As it is our aim to investigate an intermediate asymptotic coarsening regime related to the fractal structure of the cluster at $t = 0$, we should work on a (shrinking) interval of scales where, at $t = 0$, $C(r, 0)$ exhibits a power-law behavior [22]. A reasonably accurate power-law fit can be achieved at $t = 0$ on the interval $3 < r < 150$, while beyond $r = L = 150$ (the upper cutoff of the DLA cluster) finite-size effects become large. The fitting function is $c r^{-\delta}$, where $\delta = 0.30$ and $c = 0.74$. Correspondingly, the fractal dimension of our DLA clusters is $D = 2 - \delta = 1.70$, a reasonably accurate value in view of the relatively small size of our system. The inequality $r_c(t) \ll L$ puts an upper limit on the coarsening time that we can still work with. Fig. 4 shows that for

the last available time of our simulations, $t = 4900$, the ratio of r_c/L is already about 0.3. Therefore, for more reliable results we should limit ourselves by $t = 2000$, as we have already done in the fitting of $l_1(t)$.

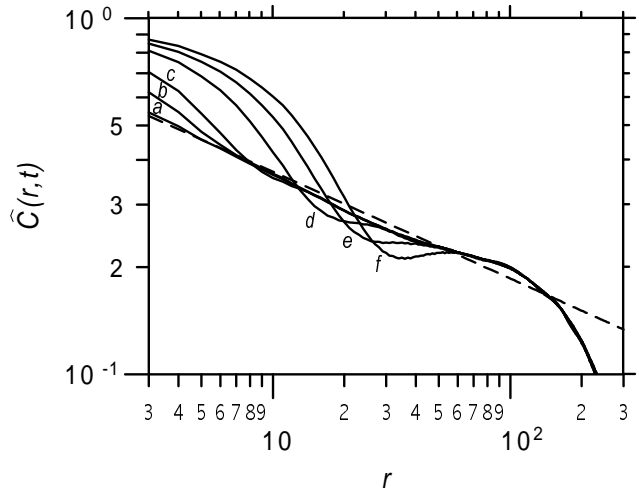


FIG. 4. Dynamics of the normalized equal-time pair correlation function $\hat{C}(r, t)$ [Eq. (8)] at time moments $t = 0$ (a), 3.65 (b), 34.7 (c), 516.5 (d), 1992 (e) and 4900 (f). The dashed line shows the power-law fit $0.74 r^{-0.30}$ on the interval $3 \leq r \leq 150$.

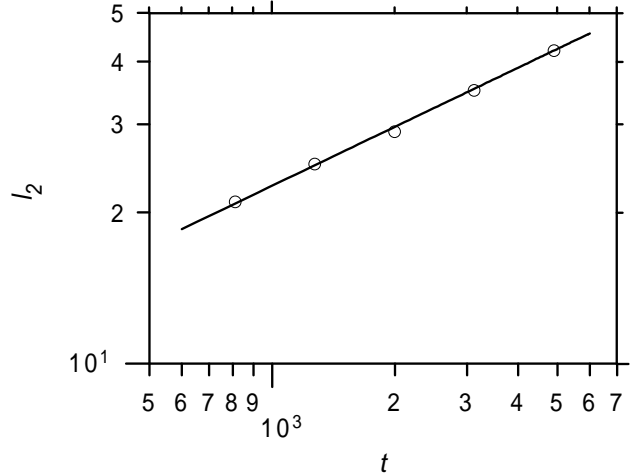


FIG. 5. The second correlation length $l_2(t)$ versus time (circles), and its fit (9) (solid line).

The normalized correlation function $\hat{C}(r, t)$ exhibits an additional dynamical length scale that appears at intermediate distances. Recall that, at sufficiently large distances, the tails of $\hat{C}(r, t)$ at different time moments coincide with $\hat{C}(r, 0)$ (see Fig. 4). We define $l_2(t)$ as the minimum value of r_1 such that for $r > r_1$ $\hat{C}(r, t)$ is less than $\hat{C}(r, 0)$ by no more than 10%. Such values of $l_2(t)$

exist only for $t > 800$, and they are shown, on the log-log plot, in Fig 5. As the available time interval in this case is quite short (less than one decade), we are forced to use the last available time $t = 4900$ and limit ourselves to a pure power-law fit:

$$l_2(t) = C_{l_2} t^\beta, \quad (9)$$

where

$$\beta = 0.39 \quad \text{and} \quad C_{l_2} = 1.5. \quad (10)$$

Though the standard deviation is small, the short time interval does not guarantee a high precision of the exponent 0.39. A big difference between the exponents α and β is, however, beyond doubt. We will interpret $l_2(t)$ as the characteristic branch *length* which serves as the time-dependent lower cutoff of the fractal “skeleton” of the coarsening cluster.

Equations (7) and (10) show an interesting relationship between l_1 and l_2 :

$$l_1 l_2^2 \propto t^{0.98}. \quad (11)$$

The exponent 0.98 is close to unity, and we will return to this observation in Section 4.

It should be noted that normalization of $C(r, t)$ at large r , which helped us to extract the second dynamical length scale, is no more artificial than the widely used normalization at $r = 0$. The only real need for *any* normalization of the equal-time pair correlation function is non-constancy of the cluster mass in time. When investigating the dynamics at small distances, it is convenient to normalize the correlation function at $r = 0$. When investigating the dynamics at large distances, it is convenient to normalize $C(r, t)$ somewhere in the tail.

B. Cluster Perimeter

Figure 6 shows the dynamics of the cluster perimeter $P(t)$. A decrease of the perimeter of a cluster under condition of (approximate) conservation of the cluster mass is a clear manifestation of coarsening. The corrected-power-law fit of $P(t)$ is

$$P(t) \approx \frac{A_P}{t^{\alpha_P} + B_P}, \quad (12)$$

where

$$\alpha_P = 0.26, \quad A_P = 7.0 \cdot 10^4 \quad \text{and} \quad B_P = 2.0. \quad (13)$$

A pure power-law fit for the last decade of time gives [9]

$$P(t) = C_P t^{-\alpha_P}, \quad (14)$$

where

$$\alpha_P = 0.20 \quad \text{and} \quad C_P = 3.5 \cdot 10^4. \quad (15)$$

The absolute values of the exponents α_P and α coincide for the same type of fit. The inverse slope of the Porod-law-part of the correlation function should indeed scale as the perimeter, because each element of interface which size is much larger than the distance r contributes independently to the correlation function [2].

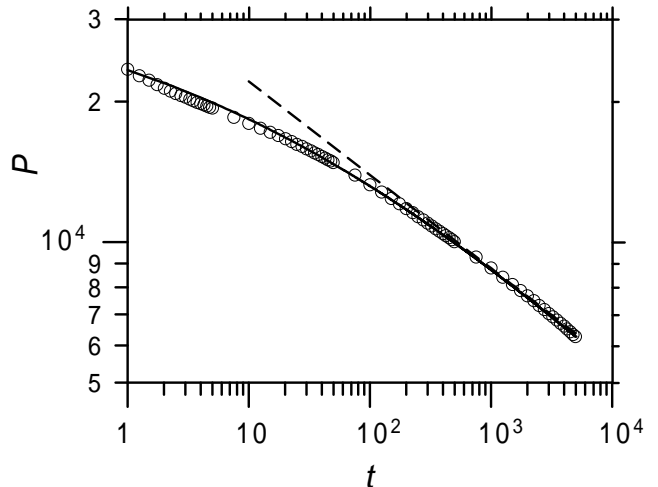


FIG. 6. Cluster perimeter $P(t)$ versus time (circles) and its fits (12) (solid line) and (14) (dashed line).

C. “Solute” Mass Outside the Cluster

Let us use, for a moment, the language of physics of liquid solutions. As *all* of the solute mass at $t = 0$ is concentrated in the DLA cluster, rapid dissolution of the solute from the cluster edge occurs first. The cluster mass will start to decrease with time. Unless the area fraction of the “fractal phase” is too small the dissolution stops, and the dissolved material precipitates back on the coarsening cluster [24]. The mass of the dissolved material decreases at this stage, while the cluster mass slowly increases, asymptotically approaching a constant value. The late stage of this regime should be qualitatively similar to Ostwald ripening, where the dynamics of the dissolved material is responsible for a correction to the Lifshitz-Slyozov scaling behavior [17].

These arguments give a qualitative explanation to our numerical results on the solute mass outside the cluster versus time, $M_s(t)$. Fig. 7 shows a log-log plot of $M_s(t)$ at sufficiently late times (the rapid “dissolution” observed at earlier times is not shown). The same figure shows two fitting functions to $M_s(t)$. A corrected-power-law fit is

$$M_s(t) = \frac{A_{M_s}}{t^\gamma + B_{M_s}}, \quad (16)$$

where

$$\gamma = 0.24, \quad A_{M_s} = 3.64 \cdot 10^4 \quad \text{and} \quad B_{M_s} = 2.4. \quad (17)$$

A pure power-law fit for $500 < t < 4900$ is

$$M_s(t) = C_{M_s} t^{-\gamma}, \quad (18)$$

where

$$\gamma = 0.16 \quad \text{and} \quad C_{M_s} = (1.45 \pm 0.02) \cdot 10^4. \quad (19)$$

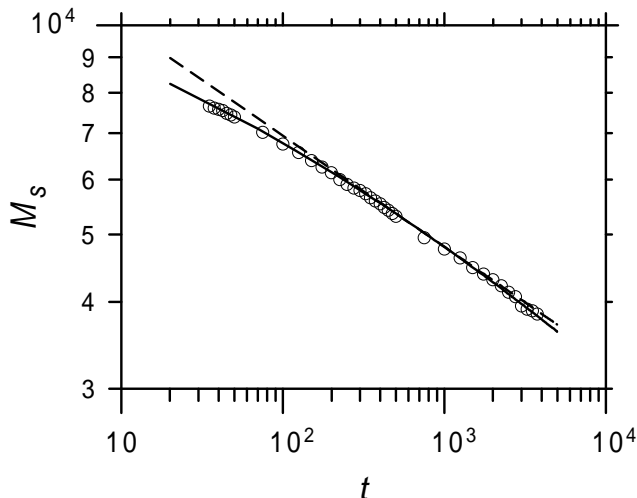


FIG. 7. Mass of “solute” outside the cluster M_s versus time (circles) and its fits (16) (solid line) and (18) (dashed line).

One can expect that the fractal coarsening dynamics look simplest (that is, corrections to dynamical scaling are small) when the cluster mass is already almost constant. This condition is only weakly satisfied in our simulations. For example, even at $t = 2000$ the solute mass outside the cluster reaches about 10% of the cluster mass. This may be the reason for the relatively large uncertainties of the numerical values of the dynamical exponents that we have found. Another possible reason is the finite size effects related to a moderate fractal range of the DLA-clusters that we used in simulations.

III. SLENDER BAR DYNAMICS

In the rest of the paper we will try to get some quantitative understanding of our numerical results. As no satisfactory theory for coarsening of FCs is available, one can try to formulate a simplified scenario and compare its predictions with simulations. The simplest possible scenario assumes dynamical scale invariance, that is the presence of a single relevant dynamical length scale [23,11]. We have seen that, in the case of CH-dynamics, this scenario disagrees with simulations. Breakdown of

dynamical scale invariance is caused by the effective locality of mass transfer which manifests itself in the (approximate) conservation of *both* the mass, *and* gyration radius of the cluster in the process of coarsening.

Looking for a scenario with broken dynamical scale invariance one should, first of all, identify the nature of the second dynamical length scale. Snapshots of the coarsening process (Fig. 1) indicate that it might be the average *length* of the cluster branches [9]. Having made this assumption, we should verify that the typical width and length of the cluster branches indeed show different dynamical scalings, the length growing faster than the width.

An important element of the scenario that we want to explore is the shrinking dynamics of a single slender bar of phase $u = 1$ (“solid”), evolving under the CH-equation (1) in the “liquid” phase $u = -1$. Special simulations show (see below) that, in the process of shrinking along its main axis, the bar acquires the shape of a dumbbell, and the “balls” at the ends of the dumbbell expand with time. In this Section we will derive scaling relations for the time-dependent parameters of the shrinking dumbbell-shaped bar, and then compare them with numerical simulations.

A. Slender bar dynamics: theoretical estimates

Our approach to the slender bar dynamics employs a modified version of the rigorous asymptotic sharp-interface theory developed for the CH-equation [2,25]. This theory (which can be called “Laplacian coarsening”) requires all characteristic length scales in the problem to be much larger than the domain wall width (which is of order unity), but much smaller than the characteristic diffusion length $l_d \sim t^{1/2}$. Under these assumptions,

- the local normal velocity of the moving interface of the bar is equal to the difference between the normal components of the gradient of the density field $\rho(\mathbf{r}, t)$ outside and inside the interface,
- the density field is represented by two harmonic functions: one outside, the other inside the bar,
- there is a Gibbs-Thomson matching condition at the moving interface and no-flux condition at the external boundary.

This formulation enforces exact conservation of the bar area in the process of coarsening. On the other hand, the condition of an infinite diffusion length is too restrictive. It is not satisfied in any of the state-of-the-art numerical simulations of phase ordering as described by the Cahn-Hilliard equation. Fortunately, it is sufficient to require in practice that the diffusion length be larger than the characteristic coarsening length(s) of the problem, and this is what we shall do.

We assume that the bar length is much larger than its width and use the aspect ratio of the bar as a large parameter. Limiting ourselves to order-of-magnitude estimates, we will assume that the density field inside the bar has already settled down, so that we can treat the bar interior simply as a region where $\rho(\mathbf{r}, t) = 1$.

What is the physical picture of the bar dynamics? Because of the large aspect ratio of the bar, the density gradient will be largest near the dumbbell ends and small elsewhere [see Eq. (20) below]. The solute, released from the bar ends, will therefore be transported to the liquid, and the bar will be shrinking along its main axis. Let us assume that the total mass of the solute outside the bar is relatively small (see below). Then most of the dissolved solute will be reabsorbed not far from the bar ends. This effectively local dynamics is the reason that the bar acquires the shape of a dumbbell. The “balls” at the ends of the shrinking dumbbell will effectively travel along the main axis of the bar like snowballs, accumulating material along their motion and growing in size.

Going over to a quantitative analysis, we consider a half-infinite bar and denote the width of its planar part by Δ . We assume that, despite the fact that the ball at the end of the dumbbell may have a complicated shape, it can still be characterized by a single time-dependent length scale $R(t)$. (Recall that what we are after is order-of-magnitude estimates, rather than a complete solution.) Let the bar be placed along the x -axis as shown in Fig. 8. In this Figure $x_0(t)$ is the time-dependent position of the bar edge (that is, the length reduction of the bar in the process of its shrinking). Introduce the polar coordinates r and ϕ with the origin at the bar end.

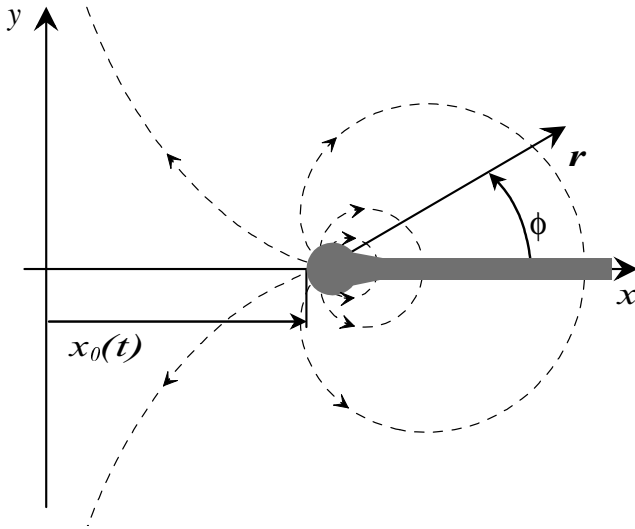


FIG. 8. Setting for the dumbbell dynamics. Dashed lines are the lines of flow calculated from Eq. (20).

The density field ρ must be a harmonic function that vanishes at the planar part of the dumbbell interface (that is, at $\phi \rightarrow 0$ and $\phi \rightarrow 2\pi$) and is of order $1/R(t)$

at the “ball” interface (for definiteness, at $\phi = \pm\pi/2$). Far enough from the bar end, $r \gg R(t)$, the bar can be considered as a thin sheet [we assume that $\Delta \ll R(t)$]. The solution of the Laplace equation for a thin sheet is elementary [27], and we can estimate the density as

$$\rho(r, \phi, t) \sim C [R(t) r]^{-1/2} \sin(\phi/2), \quad (20)$$

where C is a constant of order unity. Employing the boundary condition at the ball interface, we have extended the thin-sheet approximation to the limit of its applicability, but this can only affect the value of the constant C . Dashed lines in Fig. 8 show the streamlines of the mass flow obtained by taking the gradient of the density field (20).

Calculating the total mass of the “solute” with Eq. (20), one can see that it diverges at large r . This divergence arises because one replaces a diffusion equation by the simpler Laplace equation in the asymptotic theory of the CH-equation [2,25]. The divergence can be cured by introducing an upper cutoff R_{max} in Eq. (20). The cutoff is the smallest of the two lengths: the diffusion length $l_d \sim t^{1/2}$ and the system size L_0 .

There are two important consequences of Eq. (20). First, the density gradient $|\nabla\rho|$ is indeed largest near the bar end. As the result, the ball emits material from its edge and retreats. Second, the total mass flux to the planar part of the bar is finite, as it is proportional to $r^{-3/2}$ and therefore converges at large r along the bar edge. The second property implies that most of the solute, emitted by the bar end, is reabsorbed by the less curved part of the “ball”. Again, this requires that the solute mass outside of the bar is small, and we will return to this condition later.

Now we proceed to obtain simple scaling relations for the parameters of the shrinking half-infinite bar. Employing the (approximate) constancy of the bar mass, we have

$$x_0(t)\Delta \sim [R(t)]^2. \quad (21)$$

The mass flux out of the ball can be estimated as

$$\dot{m} \sim |\nabla\rho|_{r \sim R} R \sim [R(t)]^{-1}. \quad (22)$$

As a result of the outflow and reabsorption of this material the ball travels along the x -axis. The characteristic time τ_R it takes the ball to pass the distance comparable to its size is $\tau_R \sim m/\dot{m} \sim [R(t)]^3$, so the ball speed is

$$\dot{x}_0(t) \sim \frac{R(t)}{\tau_R} \sim [R(t)]^{-2}. \quad (23)$$

Equations (21) and (23) yield

$$\dot{x}_0(t) x_0(t) \Delta \sim 1, \quad (24)$$

which follows

$$x_0(t) \sim \Delta^{-1/2} t^{1/2}. \quad (25)$$

Then Eq. (21) yields

$$R(t) \sim \Delta^{1/4} t^{1/4} . \quad (26)$$

Therefore, shrinking of a slender bar in the CH-equation exhibits dynamical scaling with exponents 1/2 (for the bar length) and 1/4 (for the ball size). In the following we will verify Eq. (25) numerically and then employ it in our fractal coarsening scenario.

Let us return to the condition of the relative smallness of the solute mass outside the bar. Using Eq. (20) with an upper cutoff, we can estimate the solute mass outside the bar as $[R(t)]^{-1/2} R_{max}^{3/2}$. This should be much less than the ball mass:

$$[R(t)]^{-1/2} R_{max}^{3/2} \ll [R(t)]^2 . \quad (27)$$

At not too large times, $t < L_0^2$, it is the diffusion length $l_d \sim t^{1/2}$ that should be taken for the upper cutoff R_{max} . In this regime the condition (27) can be rewritten as

$$\Delta \gg t^{1/5} . \quad (28)$$

At later times, $t > L_0^2$, we should put $R_{max} \sim L_0$, and the condition (27) becomes

$$\Delta \gg L_0^{12/5} t^{-1} . \quad (29)$$

The criteria (28) and (29) coincide (by order of magnitude) in the intermediate regime $t \sim L_0^2$ and yield

$$\Delta \gg L_0^{2/5} . \quad (30)$$

Eq. (30) is the most stringent criterion, so we should require that it holds. On the other hand, we should assume that an initially rectangular bar has already developed its dumbbell shape. This requires $R(t) \gg \Delta$. Using Eq. (26), we can rewrite it as $\Delta \ll t^{1/3}$. Overall, the dumbbell scalings (25) and (26) are expected to hold when

$$L_0^{2/5} \ll \Delta \ll t^{1/3} . \quad (31)$$

B. Slender bar dynamics: numerical simulation

The dynamics of a slender bar were simulated with the same CH equation (1). We started with a rectangular-shaped bar ($u = 1$ inside the bar, $u = -1$ outside). The bar sizes were 512×8 , and the bar was placed in the center of a 1024×256 rectangular box. The CH-equation (1) was solved with periodic boundary conditions. Only one quadrant was actually simulated because of symmetry with respect to the x and y axes.

Snapshots of the bar evolution at time moments $t = 0, 8154, 26810$ and 88180 are shown in Fig. 9. They confirm the ‘‘dumbbell picture’’ qualitatively. One can see that most of the bar keeps its planar shape and constant

width. Balls are formed at the ends of the bar and travel along the bar’s main axis growing in size.

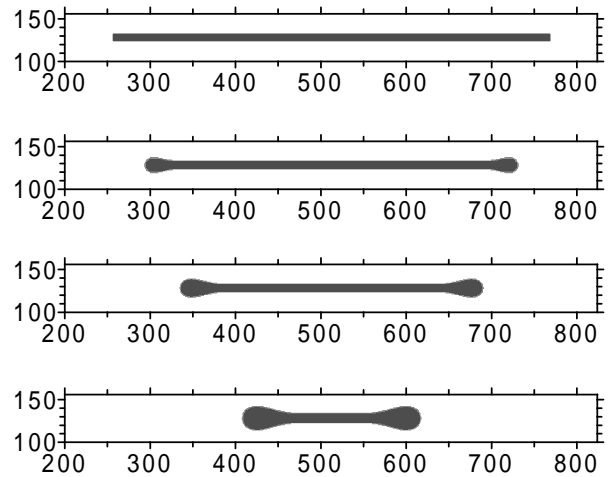


FIG. 9. Dumbbell formation and dynamics at $t = 0, 8154, 26810$ and 88180 (from top to bottom).

Fig. 10 shows the numerically obtained time-dependence of the bar length reduction $x_0(t)$. A pure power-law asymptotics of this quantity, predicted by Eq. (25), is expected to show up at very late times, when the typical size of the balls $R(t)$ becomes much larger than Δ . At intermediate times we can expect a correction of order $\Delta/R(t)$. For $\Delta = 8$ used in our simulations, this correction is significant until the latest available times $\sim 10^5$. Taking it into account, we can fit the numerical data for $x_0(t)$ by the function

$$x_0(t) = C_1 t^{1/2} + C_2 t^{1/4} . \quad (32)$$

This fit (with $C_1 = 0.6$ and $C_2 = -1.6$) and its leading term are shown separately in Fig. 10, and a good agreement is observed. Reintroducing the Δ -dependences, predicted by the theory, we can rewrite Eq. (32) as

$$x_0(t) = 1.7 (t/\Delta)^{1/2} - 0.95 (\Delta \cdot t)^{1/4} + \dots . \quad (33)$$

In the following Section we will use only the leading term of Eq. (33).

The parameters chosen for this simulation made it possible to reach the dumbbell scaling regime. Indeed, the right inequality in Eq. (31) is satisfied for any of the time moments shown in Fig. 9, except $t = 0$. Taking the system length $L_0 = 124$ (the distance between the planar part of the bar and the boundary), we see that the left inequality in Eq. (31) requires $\Delta \gg 7$. The results of the bar dynamics simulation for $\Delta = 8$ indicate that a usual (not strong) inequality is sufficient. We observed breakup of the bar into fragments for $\Delta = 4$, when this condition is violated.

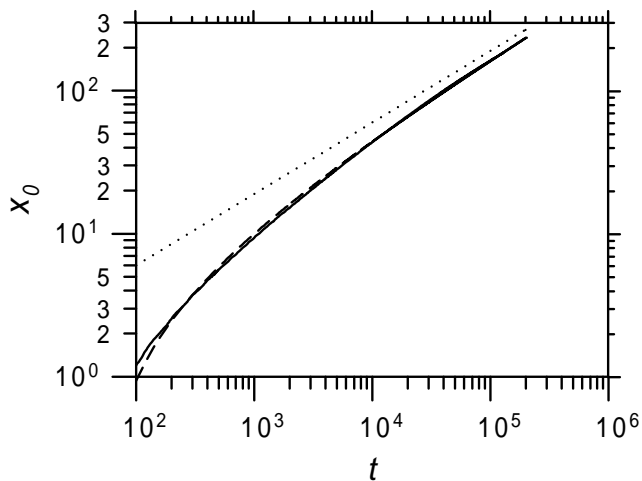


FIG. 10. The bar length reduction $x_0(t)$ versus time (solid line); fit (32) (dashed line) and its leading term (dotted line).

The results of our investigation of the slender bar dynamics are interesting in their own right. One should work with domains of a simple shape in order to understand the basics of coarsening dynamics. It is a single spherical droplet of the minority phase that usually serves as a “test object” for coarsening dynamics [1–3]. Our results show that a slender bar represents an instructive alternative. First, the slender bar dynamics exhibit locality of mass transport. Second, two different dynamical length scales appear. Neither of these two properties is present in the single droplet dynamics.

In conclusion of this section we cite earlier papers [26] where analytical solutions for the Laplacian *growth* problem were obtained in a slender bar geometry. Differences in motivation (diffusion-limited growth versus diffusion-limited coarsening) lead to important differences between these models and our model. First, the boundary condition far from the bar in Refs. [26] corresponded to a non-zero flux of material, while this flux is zero in our model. Second, papers [26] did not account for surface tension at the bar interface.

IV. “FRACTAL SKELETON” SCENARIO OF COARSENING

As it is evident from Fig. (1), a two-dimensional DLA cluster preserves, in the process of coarsening, its branching structure. We will characterize the typical cluster branch at time t by a width $a(t)$ and length $b(t)$. Later on we will identify $a(t)$ and $b(t)$ with the two time-dependent correlation distances $l_1(t)$ and $l_2(t)$, respectively. We are interested in the coarsening regime when the total mass (area) of the cluster is almost constant. Define the skeleton of the cluster (at fixed time) by tending all branches widths to zero. Coarsening of a FC in our sce-

nario involves disappearance of the shortest branches of the cluster and an increase of the width of the remaining branches so that the cluster mass remains constant. We assume that the cluster *skeleton*, rather than the cluster itself, preserves its fractal structure, with the same fractal dimension as at $t = 0$, in the process of coarsening [28]. The lower cutoff of the fractal skeleton is the typical branch *length*, and it grows with time. The upper cutoff remains constant. Another important assumption is that each individual daughter branch evolves like a single slender bar of the previous Section, until the time when its aspect ratio becomes of order unity. Then this branch rapidly shrinks and disappears, “injecting” its material into the parental branch.

Now Eq. (25) can be interpreted in the following way. Because of its shortening, the branch with the width a_0 and length b_0 has a lifetime of order

$$t_0 \sim a_0 b_0^2. \quad (34)$$

Obviously, only those branches which lifetime is larger than t will survive by time t . Therefore, at time t the typical remaining branches satisfy the scaling relation

$$a(t) b^2(t) \sim t. \quad (35)$$

The same scaling relation apparently holds for the two correlation lengths $l_1(t)$ and $l_2(t)$ [see Eq. (11)]. This indicates that $a(t)$ and $b(t)$ can indeed be identified with $l_1(t)$ and $l_2(t)$, respectively.

The total mass of the cluster can be estimated as $ab(L/b)^D$, and this quantity must be constant and equal to the initial mass M . Combining it with Eq. (35), we arrive at the following scaling relations:

$$a(t) \sim l_1(t) \sim \left(\frac{M}{L^D}\right)^{\frac{2}{D+1}} t^{\frac{D-1}{D+1}}, \quad (36)$$

$$b(t) \sim l_2(t) \sim \left(\frac{L^D}{M}\right)^{\frac{1}{D+1}} t^{\frac{1}{D+1}}. \quad (37)$$

For the cluster perimeter we obtain

$$P(t) \sim b \left(\frac{L}{b}\right)^D \sim M^{-\frac{D-1}{D+1}} L^{\frac{2D}{D+1}} t^{-\frac{D-1}{D+1}}. \quad (38)$$

The different dynamical exponents obtained for $a(t)$ and $b(t)$ explain breakdown of dynamical scale invariance. Notice that the absolute values of the exponents for $P(t)$ and $a(t)$ coincide. In the limiting case of $D = 2$ all the exponents coincide to give the Lifshitz-Slyozov value $1/3$, so that dynamical scale invariance is restored. This limiting case describes a quench through the critical point, where convoluted percolating interfaces (for which $D = 2$) are observed [18–20].

In addition, we can give a robust description of the scaling behavior of the “solute” mass outside the cluster. The “injection” processes outlined above causes undulations of the interface of the parent branches (clearly seen

in Fig. 1). In their turn, diffusion of the “solute” and surface tension tend to erase the undulations. It is natural to assume that, by time t , undulations with wavelengths smaller than $\sim t^{1/3}$ have already disappeared [29]. Hence, at time t the typical wavelength (or curvature radius) of the branch undulation is of order $t^{1/3}$. [Notice that, for $D < 2$, this curvature radius grows with time slower than $b(t)$.] The “solute” density ρ around the curved interface is of order $t^{-1/3}$ due to the Laplacian screening of “bays” by “capes”. Solute with this density will be found within a distance of the order of the diffusion length $l_d \propto t^{1/2}$ from the cluster interface. Outside of this region the density will very small. The area of this region can be estimated as

$$S_d \sim l_d^2 \left(\frac{L}{l_d} \right)^D \propto t^{\frac{2-D}{2}}. \quad (39)$$

Multiplying this quantity by the “solute” density $t^{-1/3}$, we obtain a dynamical scaling relation for the “solute” mass outside the cluster:

$$M_s \propto t^{\frac{4-3D}{6}}. \quad (40)$$

Notice that for $D = 2$ the Lifshitz-Slyozov scaling $t^{-1/3}$ for the solute mass [17] is recovered. A striking prediction of Eq. (40) is the change of sign of the dynamical exponent at $D = 4/3$. For $D < 4/3$ the “solute” mass should continue *increasing* with time until the time when the dissolving fractal degrades and the “fractal skeleton” model becomes inapplicable. It should be noted that estimate (40) is quite robust, as it is independent of most of the assumptions of the “fractal skeleton” scenario. For example, it does not use the values of the first two dynamical exponents and only assumes that they are less than $1/2$ (that is, the length and width of the branches grow in time slower than the diffusion length l_d).

Now we are in a position to compare the predictions of the “fractal skeleton” scenario with our simulations of DLA coarsening. This comparison is made in Table 1 for $D = 1.70$. The agreement is quite reasonable, in view of the uncertainty range of the exponents found numerically and simplicity of the scenario.

TABLE I. Dynamical exponents: scenario vs. simulation

Quantity	exponent	exponent	exponent
	from scenario	from corrected power-law fit	from pure power-law fit
l_1	0.26	0.26	0.20
l_2	0.37	—	0.39
P	-0.26	-0.26	-0.20
M_s	-0.18	-0.24	-0.16

V. SUMMARY AND DISCUSSION

We investigated the bulk-diffusion-controlled coarsening of DLA fractal clusters as described by the CH-equation. We observed that long-ranged correlations, introduced by the FC at $t = 0$, define a new intermediate asymptotics (in the terminology of Ref. [30]) in the coarsening dynamics: “fractal coarsening”. In order to reach this asymptotics, one should wait long enough so that quasi-equilibrium domain walls are already formed and mass transfer between the cluster and the majority phase is already weak (the cluster mass is approximately constant). On the other hand, this stage is limited at large times by finite-size effects [a finite value of $l_2(t)/L$]. This intermediate asymptotic stage is quite long (our coarsening scenario predicts that its duration is of order L^{D+1}), and it certainly deserves attention.

The main result of this work (and of the preceding Letter [9]) is breakdown of dynamical scale invariance, that is the presence of several dynamical length scales, during the bulk-diffusion-limited fractal coarsening. We identified two dynamical length scales from the evolution of the equal-time pair correlation function, and a third dynamical length scale from the evolution of the “solute” mass outside the cluster. Breakdown of dynamical scale invariance is caused by the effective locality of mass transfer which manifests itself in the *simultaneous* (approximate) conservation of the cluster mass and gyration radius in the process of coarsening. Scale-invariant mass-preserving coarsening would obviously require shrinking of the FC [11], while no shrinking is observed in this system.

Looking for a simple scenario of coarsening with a broken dynamical scale invariance, we investigated an auxiliary problem of the dynamics of a single dumbbell-shaped domain and found “unusual” dynamical exponents $1/2$ and $1/4$. Locality of mass transfer is present already in the single-dumbbell dynamics. We suggested a simple scenario of fractal coarsening in diffusion-controlled systems with a conserved order parameter. It postulates a fractal skeleton with an invariable fractal dimension and employs the dumbbell model for the dynamics of individual branches. In addition, a robust estimate of the “solute mass” exponent is obtained, and a qualitative change in the “solute mass” dynamics is predicted at $D = 4/3$. Theoretical predictions are in reasonable agreement with numerical simulations.

Much more work is needed, however, before a more complete understanding of the fractal coarsening emerges. A moderate fractal range of the DLA realizations that we worked with made it difficult to obtain sharp estimates of the dynamical exponents. More extensive numerical simulations would increase the scaling range and test the values of the dynamical exponents.

How can one put the “fractal skeleton” scenario of coarsening under additional tests? The scenario gives very definite predictions of the dynamical exponents in

terms of the (invariable) fractal dimension of the cluster skeleton. In general, fractal dimension is only one characteristic of a geometrical set. Therefore, one direct test would involve simulations of coarsening of a *different* random FC with branching structure that has the same fractal dimension as DLA. Further tests would involve simulations with random FCs having branching structures with *different* (tunable) fractal dimensions. Simulations of this type were performed in Ref. [13] for the case of edge-diffusion-controlled fractal coarsening. In our case of bulk-diffusion-controlled coarsening these tests will check, in particular, the prediction of a qualitative change in the “solute mass” dynamics at $D_{crit} = 4/3$.

Finally, a comparative investigation of different *mechanisms* of fractal coarsening (edge diffusion versus bulk diffusion, local conservation versus global conservation, etc.) is needed if we want to address the question about possible universality classes of fractal coarsening.

ACKNOWLEDGMENTS

We are very grateful to Avner Peleg and Azi Lipshtat for help, and to Roman Kris for useful discussions. This work was supported in part by a grant from Israel Science Foundation, administered by the Israel Academy of Sciences and Humanities, and by the Russian Foundation for Basic Research (grant No. 99-01-00123).

-
- [1] J.D. Gunton, M. San Miguel, and P.S. Sahni, in *Phase Transitions and Critical Phenomena*, edited by C. Domb and J.L. Lebowitz (Academic Press, New York, 1983), Vol. 8, p. 267.
- [2] A.J. Bray, *Adv. Phys.* **43**, 357 (1994).
- [3] J.S. Langer, *Rev. Mod. Phys.* **52**, 1 (1980); and in *Chance and Matter*, edited by J. Souletie, J. Vannimenus, and R. Stora (Elsevier, Amsterdam, 1987).
- [4] D.A. Kessler, J. Koplik, and H. Levine, *Adv. Phys.* **37**, 255 (1988).
- [5] E.A. Brener and V.I. Mel'nikov, *Adv. Phys.* **40**, 53 (1991).
- [6] M.B. Mineev-Weinstein, in *Fluctuations and Order. The New Synthesis* (Springer, New York, 1996), p. 239.
- [7] E. Brener, H. Müller-Krumbhaar, and D. Temkin, *Phys. Rev. E* **54**, 2714 (1996).
- [8] T. Irisawa, M. Uwaha and Y. Saito, *Europhys. Lett.* **30**, 139 (1995).
- [9] M. Conti, B. Meerson and P. Sasorov, *Phys. Rev. Lett.* **80**, 4693 (1998).
- [10] K.V. McCloud and J.V. Maher, *Physics Reports* **260**, 139 (1995).
- [11] R. Sempéré, D. Bourret, T. Woignier, J. Phalippou and R. Jullien, *Phys. Rev. Lett.* **71**, 3307 (1993).
- [12] I. Hinic, *Phys. Stat. Sol. (a)* **144**, K59, 1238 (1994).
- [13] N. Olivi-Tran, R. Thouy and R. Jullien, *J. Phys. I* **6**, 557 (1996).
- [14] P. Streitenberger, D. Förster and P. Veit, *Fractals* **5**, Suppl. Issue, 5 (1997).
- [15] G.E. Crooks, B. Ostrovsky and Y. Bar-Yam, *Phys. Rev. E* **60**, 4559 (1999).
- [16] T.A. Witten, Jr. and L.M. Sander, *Phys. Rev. Lett.* **47**, 1400 (1981).
- [17] I.M. Lifshitz and V.V. Slyozov, *J. Phys. Chem. Solids* **19**, 35 (1961).
- [18] T.M. Rogers and R.C. Desai, *Phys. Rev. B* **39**, 11956 (1989).
- [19] H. Tomita, *Prog. Theor. Phys.* **85**, **47** (1991).
- [20] C. Jeppesen and O.G. Mouritsen, *Phys. Rev. B* **47**, 14724 (1993).
- [21] D. A. Huse, *Phys. Rev. B*, **34**, 7845 (1985).
- [22] T. Vicsek, *Fractal Growth Phenomena* (World Scientific, Singapore, 1992).
- [23] H. Toyoki and K. Honda, *Phys. Lett.* **111**, 367 (1985).
- [24] The arrest of dissolution requires also that the fractal dimension of the cluster be larger than 4/3 [see Eq. (40) and the subsequent discussion].
- [25] R.L. Pego, *Proc. R. Soc. Lond. A* **422**, 261 (1989).
- [26] L.A. Turkevich and H. Scher, *Phys. Rev. Lett.* **55**, 1026 (1985); F. Family and H.G. Hentschel, *Faraday Disc. Chem. Soc.* **83**, 139 (1987).
- [27] J.D. Jackson, *Classical Electrodynamics* (Wiley, New York, 1975), p. 77.
- [28] Speaking about the fractal dimension of the skeleton, we mean its box-counting dimension [22] and assume that it is equal to the mass fractal dimension defined by the pair correlation function.
- [29] By assuming the Lifshitz-Slyozov value of the corresponding dynamical exponent, we treat the undulation dynamics as almost local (that is, independent of the global structure of the cluster and, in particular, of the fractal dimension of its skeleton).
- [30] G.I. Barenblatt, *Scaling, Self-Similarity, and Intermediate Asymptotics* (Cambridge Univ. Press, Cambridge, 1996).